arXiv:1409.4947v2 [hep-ph] 21 Jan 2016

Higher-twist mechanism and inclusive gluon production in pion-proton collisions

A. I. Ahmadov[1,2] *, C. Aydin[3] †, R. Myrzakulov[4] ‡, and O. Uzun[3] §

[1] *Fachbereich C, Bergische Universität Wuppertal, 42097 Wuppertal, Germany*

[2] *Department of Theoretical Physics, Baku State University, Z. Khalilov st. 23, AZ-1148, Baku, Azerbaijan*

[3] *Department of Physics, Karadeniz Technical University, 61080, Trabzon, Turkey and*

[4] *Eurasion International Center for Theoretical Physics and Department of General Theoretical Physics, Eurasian National University, Astana 010008, Kazakhstan*

(Dated: January 24, 2016)

Abstract

We calculate the contribution of the higher-twist Feynman diagrams to the large-p_T inclusive gluon production cross-section in πp collisions in case of the running coupling and frozen coupling approaches within perturbative and holographic QCD. The structure of infrared renormalon singularities of the higher-twist subprocess cross-section is obtained and the resummed higher-twist cross- sections (Borel sum) with the ones obtained in the framework of the frozen coupling approach and leading-twist cross-section are compared and analyzed.

PACS numbers: 12.38.-t, 13.60.Le, 14.40.Aq, 13.87.Fh

Keywords: Higher-twist, pion distribution amplitude, infrared renormalons

* E-mail: ahmadovazar@yahoo.com

† E-mail: coskun@ktu.edu.tr

‡ E-mail: rmyrzakulov@gmail.com

§ E-mail: oguzhan_deu@hotmail.com

I. INTRODUCTION

It is well known that Quantum Chromodynamics (QCD) is the fundamental theory of the strong interactions.Therefore in order to describe the structure and dynamical properties of hadrons at the amplitude level many researchers have been studying QCD. The hadronic distribution amplitude in terms of internal structure degrees of freedoms plays a crucial role in QCD process predictions.

One of the basic problems in QCD is choosing the renormalization scale in running coupling constant $\alpha_s(Q^2)$. In principle, in perturbative QCD (pQCD) calculations, the argument of the running coupling constant in both the renormalization and factorization scale Q^2 should be taken as equal to the square of the momentum transfer of a hard gluon in a corresponding Feynman diagram [1]. In the pQCD, the physical information of the inclusive gluon production is obtained efficiently; therefore, it can be directly compared to the experimental data.

It should be noted that problem the existence of the higher-twist contribution is not yet settled. Also it is necessary to study the difference in the leading-twist results for the frozen and running coupling constant approaches and compare it with that of the higher-twist.

The aim of this study is calculation and analysis of the inclusive gluon production in the pion-proton collisions using the frozen and running coupling constant approaches. Using this approaches, the higher twist effects have been already calculated by many authors [2–16].

The calculation and analysis of the higher-twist effects on the dependence of the pion distribution amplitude in inclusive gluon production at πp collision within holhographic and pQCD approaches are the interesting research problems. In our previously study [12], using the principle of maximum conformality (PMC) and Brodsky-Lepage-Mackenzie (BLM) approaches, we have calculated the contribution of the higher-twist mechanism to the large-p_T inclusive gluon production cross section in πp collisions [12]. In this study, we compute the contribution of the higher-twist effects to an inclusive gluon production cross-section by using various pion distribution amplitudes from holographic and pQCD, and applying the frozen and running coupling [17] constant approaches in order to compute the effects of the infrared renormalons. We also estimate and perform comparisons of the leading and the higher-twist contributions. Studying various properties of the hadron infrared renormalon effects in detail is one of the essential and actual problems in the pQCD [18–26]. This

approach was also employed before [5–11] to calculate the inclusive meson production in pp and $\gamma\gamma$ collisions.

The contents of the paper is as follows. The related formulas for the calculation of the contributions of the higher-twist and leading-twist diagrams are provided in the next section. The formulas and analysis of the higher twist effects on the dependence of the pion distribution amplitudes by the running coupling constant approach are presented in Section III, and the numerical results for the cross-section and discussion of the dependence of the cross-section on the pion distribution amplitudes are presented in Section IV. Finally, our conclusions and the highlights of the study are listed in Section V.

II. HIGHER-TWIST AND LEADING-TWIST CONTRIBUTIONS TO INCLUSIVE GLUON PRODUCTION

The higher-twist Feynman diagrams for the inclusive gluon production in the pion-proton collision $\pi p \to gX$ are shown in Fig.1. For the process $\pi p \to gX$, we write invariant amplitude as in the form (as called by Brodsky-Lepage formula [27])

$$M(\hat{s},\hat{t}) = \int_0^1 dx_1 \int_0^1 dx_2 \delta(1-x_1-x_2)\Phi_M(x_1,x_2,Q^2)T_H(x_1,x_2;Q^2,\mu_R^2,\mu_F^2) \tag{2.1}$$

where T_H is the sum of the graphs contributing to the hard-scattering part of the subprocess. For the higher-twist, the subprocess is taken as $\pi q_p \to gq$, which contributes to $\pi p \to gX$, where q_p is a constituent of the initial proton target. As seen from Fig.1, the processes $\pi^+ p \to gX$ and $\pi^- p \to gX$ arise from subprocesses as $\pi^+ d_p \to gu$ and $\pi^- u_p \to gd$, respectively.

The production of the hadronic gluon in the large transverse momentum is available at the high energy, especially at the Large Hadron Collider. Finally, hadronic gluon is a product of the hard-scattering processes, before hadronization. In the final state, this hadronic gluon is fragmented to hadron. The main dynamical properties of the gluon, which carried one part of the four momentum, are close to the parent parton. In order to understand the parton kinematics one should consider the gluon production process [28]. The higher-twist cross-section for $\pi p \to gX$ process has the form:

$$E\frac{d\sigma}{d^3p}(\pi p \to gX) = \int_0^1 dx \delta(\hat{s}+\hat{t}+\hat{u})\hat{s}G_{q/p}(x,Q^2)\frac{1}{\pi}\frac{d\sigma}{d\hat{t}}(\pi q_p \to gq), \tag{2.2}$$

where $G_{q/p}(x,Q^2)$ is the quark distribution function inside a proton.

For higher-twist subprocess $\pi q_p \to gq$, the Mandelstam invariant variables are written in the form:

$$\hat{s} = (p_1 + p_g)^2 = (p_2 + p_\pi)^2, \quad \hat{t} = (p_g - p_\pi)^2, \quad \hat{u} = (p_1 - p_\pi)^2. \tag{2.3}$$

Then the parton-level cross-section within running coupling constant method becomes

$$\frac{d\sigma}{d\hat{t}}(\pi q_p \to gq) = \frac{256\pi^2}{81\hat{s}^2} \left[D(\hat{s}, \hat{u})\right]^2 \left(-\frac{\hat{t}}{\hat{s}^2} - \frac{\hat{t}}{\hat{u}^2}\right), \tag{2.4}$$

where

$$D(\hat{s}, \hat{u}) = \int_0^1 dx \alpha_s^{3/2}(Q_1^2) \left[\frac{\Phi_\pi(x, Q_1^2)}{x(1-x)}\right] + \int_0^1 dx \alpha_s^{3/2}(Q_2^2) \left[\frac{\Phi_\pi(x, Q_2^2)}{x(1-x)}\right]. \tag{2.5}$$

By the way, it must be denoted that as a special case we can directly get the result [29] from Eq(2.4) by the applying the frozen coupling constant approximation.

If we use the BLM approach for Fig.1 the transfer momentum of the hard gluon for s and u channels get the form

$$Q_1^2 = (1-x)\hat{s} \quad \text{and} \quad Q_2^2 = -x\hat{u}, \tag{2.6}$$

respectively.

In the soft regions $x \to 0$ and $x \to 1$ (for u and s channels), integrals (2.5) diverge, therefore in these regions for their calculations some regularization methods of $\alpha_s(Q^2)$ are needed. One of the simple method is called frozen coupling constant approximation for the regularization these singularity.

Although the frozen QCD coupling constant was introduced a long time ago, it is also interesting and important in these days [30–38]. The origin of it comes from the divergent infrared behavior of the well-known renormalization group expression for α_s. For this reason, it is used as a constant in the infrared domain. Another reason for introducing the frozen coupling is the pQCD coupling. Also, the effects of running α_s should be taken into account in all calculations. However, it makes some QCD calculations very difficult. If we want to estimate it approximately, it can be very convenient to use some effective coupling which minimizes the running of α_s in the perturbative region. For getting an agreement with experimental data, the values of the frozen coupling are usually fixed from purely phenomenological considerations. The frozen coupling is frequently used in combination with other phenomenological parameters to describe hadronic processes. We can come across fixed α_s very often in various calculations done in the framework of the leading logarithmic approximation where most important logarithmic contributions are totally resummed

while α_s considered as fixed parameter and its argument is set off a posteriori from physical considerations. The solution of the Schwinger-Dyson equations can be also another method for investigating the infrared behavior of the gluon and ghost propagators and for the running coupling constant at low energies [39]. Although early studies of the Schwinger-Dyson equations for the gluon propagator are very singular in the infrared [40–42], other studies found infrared finite propagators. For example, in Ref. [43] the gluon acquires a dynamical mass m_g^2, and the other is extensively discussed in Refs. [44, 45] when the gluon propagator goes to zero when the momentum $Q^2 \to 0$. In both cases, the freezing of coupling constant appears in the infrared. In the case where squared momentum of a hard gluon gets the form $Q^2 \to Q^2 + m_g^2$, for running coupling constant leads to $\alpha_s(Q^2) \to \alpha_s(Q^2 + m_g^2)$. Here m_g^2 is interpreted as an effective dynamical gluon mass or fictitious mass of gluon. By frozen coupling constant approach for squared of transfer momentum of the hard gluon in single meson photoproduction, $\gamma p \to MX$ is taken as $Q_1^2 = \hat{s}/2$ and $Q_2^2 = -\hat{u}/2$ [13]. Additionally, we also come across other physical properties of frozen coupling constant in the confinement mechanism suggested in Refs. [46, 47] as $(1+1)$ dimensional Quantum Electrodyanamics .

There are few forms of the pion distribution amplitude available in the literature. In the present numerical calculations, we use several choices, such as the asymptotic distribution amplitude derived in pQCD evalution [48], the Vega-Schmidt-Branz-Gutsche-Lyubovitskij (VSBGL) distribution amplitude [49], distribution amplitudes predicted by AdS/CFT [50, 51], the Chernyak-Zhitnitsky(CZ) [52], the Bakulev-Mikhailov-Stefanis (BMS) [53, 54] and pion distribution amplitudes in which Gegenbauer coefficients C_2 and C_4 are extracted from BELLE experiment [55, 56]:

$$\Phi_{asy}(x, Q^2 \to \infty) = \sqrt{3} f_\pi x(1-x), \tag{2.7}$$

$$\Phi^{hol}_{VSBGL}(x, \mu_0^2) = \frac{A_1 k_1}{2\pi} \sqrt{x(1-x)} exp\left(-\frac{m^2}{2k_1^2 x(1-x)}\right), \tag{2.8}$$

$$\Phi^{hol}(x, \mu_0^2) = \frac{4}{\sqrt{3}\pi} f_\pi \sqrt{x(1-x)}, \tag{2.9}$$

$$\Phi_{CZ}(x, \mu_0^2) = \Phi_{asy}(x) \left[C_0^{3/2}(2x-1) + \frac{2}{3} C_2^{3/2}(2x-1)\right], \tag{2.10}$$

$$\Phi_{BMS}(x, \mu_0^2) = \Phi_{asy}(x) \left[C_0^{3/2}(2x-1) + 0.20 C_2^{3/2}(2x-1) - 0.14 C_4^{3/2}(2x-1)\right], \tag{2.11}$$

$$\Phi_{BELLE}(x, \mu_0^2) = \Phi_{asy}(x) \left[C_0^{3/2}(2x-1) + 0.12 C_2^{3/2}(2x-1) + 0.08 C_4^{3/2}(2x-1)\right], \tag{2.12}$$

here $C_n^{\lambda}(2x-1)$ are Gegenbauer polynomials.

Substituting Eq.(2.4) into Eq.(2.2), then the differential cross- section for the process $\pi p \to gX$ takes the form [29]

$$E\frac{d\sigma}{d^3p}(\pi p \to gX) = \frac{s}{s+u} x G_{q/p}(x,Q^2)\frac{256\pi}{81\hat{s}^2}\left[D(\hat{s},\hat{u})\right]^2\left(-\frac{\hat{t}}{\hat{s}^2}-\frac{\hat{t}}{\hat{u}^2}\right). \tag{2.13}$$

It should be noted that, as seen from Eqs.(2.4) and (2.13), the higher-twist cross-section is linear with respect to $\hat{t}$, so the cross-section vanishes, if the scattering angle between the final gluon and incident pion is approximately equal to zero. From Eq.(2.13), we see that the higher-twist cross-section proportional to $\hat{s}^{-3}$, which is equivalent to the higher-twist contributions to the $\pi p \to gX$ cross-section have the form of $p_T^{-6} f(x_F, x_T)$.

In the expression Eq.(2.6), we fixed the variable x by taking it as mean value. So, average values for x we take $\overline{x} = 1/2$. Thus, for the calculations higher-twist cross-sections within frozen coupling constant approach we substitute $\overline{Q}^2 = \hat{s}/2$ and $\overline{Q}^2 = -\hat{u}/2$ in Eq.(2.13) for the transfer momentum of the hard gluon, respectively.

The extracting of higher-twist contribution from the inclusive gluon production cross-section is also complicated. One can also consider the comparison of higher-twist corrections with leading-twist contributions. For the leading-twist subprocess in the inclusive gluon production, we take $q\bar{q} \to g\gamma$ as a subprocess of the quark-antiquark annihilation. The differential cross-section for subprocess $q\bar{q} \to g\gamma$ is

$$\frac{d\sigma}{d\hat{t}}(q\bar{q} \to g\gamma) = \frac{8}{9}\pi\alpha_E\frac{e_q^2}{\hat{s}^2}\left(\alpha_s(-\hat{u})\frac{\hat{t}}{\hat{u}} + \alpha_s(-\hat{t})\frac{\hat{u}}{\hat{t}}\right). \tag{2.14}$$

As is seen from Eq.(2.14), leading-twist cross-section strongly depends of the running coupling constant where the running coupling constant depends on the transfer momentum. However, running coupling constant depends on the channels of the process. Here running coupling have been evaluated in the momentum subtraction scheme, for momentum scales u and t, which define the off-shell momenta carried by the quark propagators.

The leading-twist cross-section for production of inclusive gluon is [57]

$$\Sigma_M^{LT} \equiv E\frac{d\sigma}{d^3p}(\pi p \to gX) = \int_0^1 dx_1 \int_0^1 dx_2 \delta(\hat{s}+\hat{t}+\hat{u}) G_{\overline{q}/M}(x_1,Q_1^2) G_{q/p}(x_2,Q_2^2)\frac{\hat{s}}{\pi}\frac{d\sigma}{d\hat{t}}(q\bar{q} \to g\gamma), \tag{2.15}$$

where

$$\hat{s} = x_1 x_2 s,\ \hat{t} = x_1 t,\ \hat{u} = x_2 u.$$

Finally, leading-twist contribution to the large-p_T gluon production cross-section in the process $\pi p \to gX$ is

$$\Sigma_M^{LT} \equiv E\frac{d\sigma}{d^3p}(\pi p \to gX) = \int_0^1 dx_1 \frac{1}{x_1 s + u} G_{\overline{q}/M}(x_1, Q_1^2) G_{q/p}(1-x_1, Q_2^2) \frac{\hat{s}}{\pi}\frac{d\sigma}{d\hat{t}}(q\bar{q} \to g\gamma). \tag{2.16}$$

III. HIGHER TWIST MECHANISM WITHIN PERTURBATIVE AND HOLOGRAPHIC QCD AND THE ROLE INFRARED RENORMALONS

The main object of this study is the calculations of the higher- twist cross-section with running coupling constant approach within holographic and pQCD and renormalon effect's contribution to the cross-section, and also comparisons between higher-twist cross- sections which are calculated by the running coupling constant method and the principle maximum conformality approach. It should be noted that, in the exclusive processes, the coupling constant α_s runs not only due to the loop integration but also the integration in the process amplitude over the light-cone momentum fraction of hadron constituents. Therefore, it is worth noting that the renormalization scale according to Fig.1 should be chosen equal to $\mu_{R_1}^2 = Q_1^2 = (1-x)\hat{s}$, and $\mu_{R_2}^2 = Q_2^2 = -x\hat{u}$. The integral in Eq.(2.5) in the framework of the running coupling approach takes the form

$$D(\mu_R^2) = \int_0^1 \frac{\alpha_s^{3/2}((1-x)\hat{s})\Phi_M(x,\mu_F^2)dx}{x(1-x)} + \int_0^1 \frac{\alpha_s^{3/2}(-x\hat{u})\Phi_M(x,\mu_F^2)dx}{x(1-x)}. \tag{3.1}$$

At the leading order of pQCD calculations the hard scattering amplitude $T_H(x_1, x_2; Q^2, \mu_R^2, \mu_F^2)$ does not depend on the factorization scale μ_F^2, but strongly depends on μ_R^2. The one-loop QCD correction to the hard scattering amplitude $T_H(x_1, x_2; Q^2, \mu_R^2, \mu_F^2)$ generates its explicit dependence on the scales μ_F^2 and μ_R^2 . Also, it should be noted that the scales μ_F^2 and μ_R^2 are independent of each other so they can be chosen autonomously.

As we noted above in the regions $x \to 0$ and $x \to 1$ the integral (3.1) diverges, because in this region the running coupling constants $\alpha_s((1-x)\hat{s})$ and $\alpha_s(-x\hat{u})$ have the infrared singularity. In other words, the singularity of the integrand of x=0 and x=1 is due to only by $\alpha_s((1-x)\hat{s})$ and $\alpha_s(-x\hat{u})$. Thus, for the regularization of the integral, by expressing the running coupling at scaling variable $\alpha_s(\mu_R^2)$, we use renormalization group equation with the fixed $\alpha_s(\hat{s})$ and $\alpha_s(-\hat{u})$ for s and u channels, respectively. The solution of renormalization group equation for the running coupling $\alpha \equiv \alpha_s/\pi$ is in the form [24]

$$\frac{\alpha(\lambda)}{\alpha} = \left[1 + \alpha\frac{\beta_0}{4}\ln\lambda\right]^{-1}. \tag{3.2}$$

Then, for $\alpha_s((1-x)\hat{s})$, we get

$$\alpha((1-x)s) = \frac{\alpha_s}{1 + ln(1-x)/t} \tag{3.3}$$

where $t = 4\pi/\alpha_s(Q^2)\beta_0 = 4/\alpha\beta_0$.

If we insert Eq.(3.3) into Eq.(3.1), we obtain

$$D(\hat{s},\hat{u}) = \int_0^1 dx\frac{\alpha_s^{3/2}((1-x)\hat{s})\Phi_\pi(x,Q_1^2)}{x(1-x)} + \int_0^1 dx\frac{\alpha_s^{3/2}(-x\hat{u})\Phi_\pi(x,Q_2^2)}{x(1-x)}$$

$$= \alpha_s^{3/2}(\hat{s})t_1^{3/2}\int_0^1 dx\frac{\Phi_\pi(x,Q_1^2)}{x(1-x)(t_1+\ln\lambda_1)^{3/2}} + \alpha_s^{3/2}(-\hat{u})t_2^{3/2}\int_0^1 dx\frac{\Phi_\pi(x,Q_2^2)}{x(1-x)(t_2+\ln\lambda_2)^{3/2}} \tag{3.4}$$

where $t_1 = 4\pi/\alpha_s(\hat{s})\beta_0$ and $t_2 = 4\pi/\alpha_s(-\hat{u})\beta_0$.

Although the integral (3.4) still has singularity, this expression can be transformed to a more convenient form by the change of variable as, $z = \ln\lambda$. Then the singularity in (3.4) disappears and we obtain

$$D(\hat{s},\hat{u}) = \alpha_s^{3/2}(\hat{s})t_1^{3/2}\int_0^1 \frac{\Phi_\pi(x,Q_1^2)dx}{x(1-x)(t_1+z_1)^{3/2}} + \alpha_s^{3/2}(-\hat{u})t_2^{3/2}\int_0^1 \frac{\Phi_\pi(x,Q_2^2)dx}{x(1-x)(t_2+z_2)^{3/2}}. \tag{3.5}$$

After applying the integral representation of $1/(t+z)^\nu$ [58, 59],

$$\frac{1}{(t+z)^\nu} = \frac{1}{\Gamma(\nu)}\int_0^\infty e^{-(t+z)u}u^{\nu-1}du, Re\nu > 0 \tag{3.6}$$

Equation (3.5) becomes

$$D(\hat{s},\hat{u}) = \frac{\alpha_s^{3/2}(-\hat{s})t_1^{3/2}}{\Gamma(\frac{3}{2})}\int_0^1\int_0^\infty \frac{\Phi_\pi(x,Q_1^2)e^{-(t_1+z_1)u}u^{1/2}dudx}{x(1-x)} +$$
$$+\frac{\alpha_s^{3/2}(-\hat{u})t_2^{3/2}}{\Gamma(\frac{3}{2})}\int_0^1\int_0^\infty \frac{\Phi_\pi(x,Q_2^2)e^{-(t_2+z_2)u}u^{1/2}dudx}{x(1-x)}, \tag{3.7}$$

Then the Eq.(3.7) can be written, for $\Phi^{hol}(x,Q^2)$, as

$$D(\hat{s},\hat{u}) = \frac{32\sqrt{\pi}f_\pi}{\beta_0\sqrt{3\beta_0}\Gamma(\frac{3}{2})}\int_0^\infty due^{-t_1u}u^{1/2}B\left(\frac{1}{2},\frac{1}{2}-u\right) +$$
$$+\frac{32\sqrt{\pi}f_\pi}{\beta_0\sqrt{3\beta_0}\Gamma(\frac{3}{2})}\int_0^\infty due^{-t_2u}u^{1/2}B\left(\frac{1}{2},\frac{1}{2}-u\right), \tag{3.8}$$

for $\Phi_{asy}(x,Q^2\to\infty)$ distribution amplitude, as

$$D(\hat{s},\hat{u})=\frac{8\pi\sqrt{3\pi}f_\pi}{\beta_0\sqrt{\beta_0}\Gamma(\frac{3}{2})}\int_0^\infty due^{-t_1u}\left[\frac{u^{1/2}}{1-u}\right]+\frac{8\pi\sqrt{3\pi}f_\pi}{\beta_0\sqrt{\beta_0}\Gamma(\frac{3}{2})}\int_0^\infty due^{-t_2u}\left[\frac{u^{1/2}}{1-u}\right], \qquad (3.9)$$

for $\Phi_{CZ}(x,Q^2)$ distribution amplitude, as

$$\begin{aligned}D(\hat{s},\hat{u}) \;=\; & \frac{8\pi\sqrt{3\pi}f_\pi}{\beta_0\sqrt{\beta_0}\Gamma(\frac{3}{2})}\int_0^\infty due^{-t_1u}u^{1/2}\left[\frac{1}{1-u}+0.84\left[\frac{4}{1-u}-\frac{20}{2-u}+\frac{20}{3-u}\right]\left(\frac{\alpha_s(Q_1^2)}{\alpha_s(\mu_0^2)}\right)^{\frac{50}{81}}\right]+\\ & \frac{8\pi\sqrt{3\pi}f_\pi}{\beta_0\sqrt{\beta_0}\Gamma(\frac{3}{2})}\int_0^\infty due^{-t_2u}u^{1/2}\left[\frac{1}{1-u}+0.84\left[\frac{4}{1-u}-\frac{20}{2-u}+\frac{20}{3-u}\right]\left(\frac{\alpha_s(Q_2^2)}{\alpha_s(\mu_0^2)}\right)^{\frac{50}{81}}\right].\end{aligned} \qquad (3.10)$$

and for $\Phi_{BMS}(x,Q^2)$ distribution amplitude, as

$$\begin{aligned}D(\hat{s},\hat{u}) \;=\; & \frac{8\pi\sqrt{3\pi}f_\pi}{\beta_0\sqrt{\beta_0}\Gamma(\frac{3}{2})}\int_0^\infty due^{-t_1u}u^{1/2}\left[\frac{1}{1-u}+0.30\left[\frac{4}{1-u}-\frac{20}{2-u}+\frac{20}{3-u}\right]\left(\frac{\alpha_s(Q_1^2)}{\alpha_s(\mu_0^2)}\right)^{\frac{50}{81}}-\right.\\ & \left.0.2625\left[\frac{8}{1-u}-\frac{120}{2-u}+\frac{560}{3-u}-\frac{1112}{4-u}+\frac{1008}{5-u}-\frac{336}{6-u}\right]\left(\frac{\alpha_s(Q_1^2)}{\alpha_s(\mu_0^2)}\right)^{364/405}\right]+\\ & \frac{8\pi\sqrt{3\pi}f_\pi}{\beta_0\sqrt{\beta_0}\Gamma(\frac{3}{2})}\int_0^\infty due^{-t_2u}u^{1/2}\left[\frac{1}{1-u}+0.30\left[\frac{4}{1-u}-\frac{20}{2-u}+\frac{20}{3-u}\right]\left(\frac{\alpha_s(Q_2^2)}{\alpha_s(\mu_0^2)}\right)^{\frac{50}{81}}-\right.\\ & \left.0.2625\left[\frac{8}{1-u}-\frac{120}{2-u}+\frac{560}{3-u}-\frac{1112}{4-u}+\frac{1008}{5-u}-\frac{336}{6-u}\right]\left(\frac{\alpha_s(Q_2^2)}{\alpha_s(\mu_0^2)}\right)^{364/405}\right].\end{aligned} \qquad (3.11)$$

where $B(\alpha,\beta)$ is Beta function and u is the Borel parameter.

The structure of the infrared renormalon poles in Eqs.(3.8)-(3.11) strongly depend on the distribution amplitudes of the pion. The integrals in Eqs.(3.8)-(3.11) are divergent.Therefore there are regularized by means of the principal value prescription by using running coupling constant. In the subsequent calculation and figures the higher-twist cross sections obtained using the running coupling and frozen coupling constant approaches are denoted by $(\Sigma_g^{HT})^{res}$ and $(\Sigma_g^{HT})^0$, respectively.

IV. NUMERICAL RESULTS AND DISCUSSION

We discuss the numerical results for higher-twist and renormalon mechanism with higher-twist contributions calculated in the context of the running and frozen coupling approaches on the dependence of the chosen pion distributions amplitudes in the inclusive gluon production process. For the numerical calculations, we take supprocess $\pi^+d_p\to gu$ and $\pi^-u_p\to gd$ for $\pi^+p\to gX$ and $\pi^-p\to gX$ process, respectively.

Inclusive direct gluon production represents a significant test case in which higher-twist terms dominate those of leading-twist in certain kinematic domains. For the dominant leading-twist subprocess for the gluon production, we take the quark-antiquark annihilation $q\bar{q} \to \gamma g$. In the numerical calculations, for the quark distribution functions inside the pion and proton we used expressions as given in Refs. [60, 61], respectively.

Results obtained in our calculations are visualized in Figs. 2-23. In all figures we represent the choice of pion distribution amplitudes Eqs.(2.7)-(2.12) by different line types: $\Phi_{asy}(x)$ as solid black line, $\Phi^{hol}(x)$ as dashed red line, $\Phi^{hol}_{VSBGL}(x)$ as dotted blue line, $\Phi_{CZ}(x,Q^2)$ as dash-dot magenta line, $\Phi_{BMS}(x,Q^2)$ as dash-double dot olive line, and $\Phi_{BELLE}(x,Q^2)$ as short dash navy line. Firstly, it is very interesting to compare the higher-twist cross sections obtained within holographic QCD with ones obtained within the perturbative QCD and also with the leading-twist cross-section. In Figs. 2 and 3, we show higher-twist cross-sections $(\Sigma_g^{HT})^0, (\Sigma_g^{HT})^{res}$ calculated in the context of the frozen (frozen cross-section) and running coupling constant (resummed cross-section) approaches as a function of the gluon transverse momentum p_T for the pion distribution amplitudes presented in Eqs.(2.6)-(2.11) at $y = 0$. It is seen from Figs. 2 and 3 that the higher-twist cross-section is monotonically decreasing with an increase in the transverse momentum of the gluon. In the region $2\ GeV/c < p_T < 30\ GeV/c$, the resummed cross-sections of the process $\pi^+ p \to gX$ decrease in the range between $3.172 \cdot 10^{-6} \mu b/GeV^2$ to $4.912 \cdot 10^{-16} \mu b/GeV^2$. In Figs. 4-7, we show $(\Sigma_g^{HT})^{res}/(\Sigma_g^{HT})^0$,$(\Sigma_g^{HT})^{res}/(\Sigma_g^{HT})^{PMC}$, $(\Sigma_g^{HT})^0/(\Sigma_g^{LT})$ and $(\Sigma_g^{HT})^{res}/(\Sigma_g^{LT})$ for the process $\pi^+ p \to gX$ as a function of p_T for the pion distribution amplitudes presented in Eqs.(2.7)-(2.12) at $y = 0$. We see in Fig. 4, that in the region $15\ GeV/c < p_T < 22\ GeV/c$, the ratio $(\Sigma_g^{HT})^{res}/(\Sigma_g^{HT})^0$ for $\Phi_{CZ}(x,Q^2)$ is enhanced by about two orders of magnitude relative to one for $\Phi_{asy}(x)$. However, the enhancement is one order of magnitude for $\Phi^{hol}(x)$ and half an order for $\Phi_{BMS}(x,Q^2)$ and $\Phi_{BELLE}(x,Q^2)$ pion distribution amplitudes. For the present the distinction between running coupling constant and principle maximum conformality approaches in Fig. 5 is shown where the $(\Sigma_g^{HT})^{res}/(\Sigma_g^{HT})^{PMC}$ ratio of higher-twist cross-sections is calculated by running coupling constant method and principle maximum conformality approach as a function of the transverse momentum of the gluon p_T. For full analysis in Table I we present numerically values of the ratio $(\Sigma_g^{HT})^{res}/(\Sigma_g^{HT})^{PMC}$ as a function of the transverse momentum of the gluon p_T. In Figs.6 and 7, we show the dependence of the ratios $(\Sigma_g^{HT})^0/(\Sigma_g^{LT})$ and $(\Sigma_g^{HT})^{res}/(\Sigma_g^{LT})$ on the gluon p_T for the pion distribution ampli-

tudes presented in Eqs.(2.6)-(2.11). It is seen that in the region 10 $GeV/c < p_T < 25$ GeV/c leading-twist cross-sections are enhanced by about four orders of magnitude relative to the higher-twist cross-sections calculated in the frozen coupling constant approach, but in some regions they are enhanced by about three orders of magnitude relative to the resummed higher-twist cross-section for $\Phi_{CZ}(x,Q^2)$. In Figs. 8-11, we have depicted higher-twist cross-sections $(\Sigma_g^{HT})^0$, $(\Sigma_g^{HT})^{res}$ and ratios $(\Sigma_g^{HT})^{res}/(\Sigma_g^{HT})^0$, $(\Sigma_g^{HT})^0/(\Sigma_g^{LT})$ and $(\Sigma_g^{HT})^{res}/(\Sigma_g^{LT})$ as a function of p_T at $\sqrt{s} = 62.4$ GeV for the process $\pi^- p \to gX$. In Figs. 8 and 9, we display the dependence of higher-twist cross-sections $(\Sigma_g^{HT})^0$, $(\Sigma_g^{HT})^{res}$ as a function of p_T for pion distribution amplitudes presented in Eqs.(2.7)-(2.12) at $y = 0$. From the figures, we see that the higher-twist cross-section is monotonically decreasing with an increase of p_T. In this process, in the region 2 $GeV/c < p_T < 30$ GeV/c, the resummed cross-sections decrease in the range between $4.556 \cdot 10^{-6} \mu b/GeV^2$ and $6.056 \cdot 10^{-14} \mu b/GeV^2$. In Figs. 10 and 11, we display the dependence of the ratios $(\Sigma_g^{HT})^0/(\Sigma_g^{LT})$ and $(\Sigma_g^{HT})^{res}/(\Sigma_g^{LT})$ for the process $\pi^- p \to gX$ as a function of p_T for the pion distribution amplitudes presented in Eqs.(2.7)-(2.12) at $y = 0$. It should be noted, that ratio $(\Sigma_g^{HT})^{res}/(\Sigma_g^{HT})^0$ for the $\pi^+ p \to gX$ process is identical to the ratio $(\Sigma_g^{HT})^{res}/(\Sigma_g^{HT})^0$ for the process $\pi^- p \to gX$. In Fig.10, we show the dependence of the ratio $(\Sigma_g^{HT})^{res}/(\Sigma_g^{LT})$, as a function of p_T for the pion distribution amplitudes presented in Eqs.(2.7)-(2.12) at $y = 0$. We also see from the figure that in the region 10 $GeV/c < p_T < 30$ GeV/c, leading-twist cross-sections are enhanced by about three orders of magnitude relative to the frozen cross-sections for $\Phi^{hol}(x)$, $\Phi_{asy}(x)$, $\Phi_{CZ}(x,Q^2)$, $\Phi_{BMS}(x,Q^2)$ and $\Phi_{BELLE}(x,Q^2)$ at $y = 0$. But the enhancement is about 4 orders of magnitude relative to the frozen cross section for $\Phi_{VSBGL}^{hol}(x)$ distribution amplitude.

From Figs. 12-19, the dependences of higher-twist cross-sections $(\Sigma_g^{HT})^0$, $(\Sigma_g^{HT})^{res}$, ratios $(\Sigma_g^{HT})^{res}/(\Sigma_g^{HT})^0$, $(\Sigma_g^{HT})^{res}/(\Sigma_g^{HT})^{PMC}$ and $(\Sigma_g^{HT})^{res}/(\Sigma_g^{LT})$ are shown for the processes $\pi^+ p \to \gamma X$ and $\pi^- p \to \gamma X$ as a function of the rapidity of the gluon y at the transverse momentum of the gluon $p_T = 4.9$ GeV/c. It is seen from figures in Figs.12 and 13, that frozen and resummed cross sections for all distribution amplitudes of pion have two maxima, where the first maximum is approximately at the point $y = -2$ and second maximum is approximately at the point $y = 2$. But, the leading-twist cross- section only has one maximum at $y = 1.5$. Notice that the distribution amplitude of frozen and resummed cross-sections for $\Phi_{CZ}(x,Q^2)$ are enhanced by about half and two orders of magnitude relative to all other distribution amplitudes. In Figs.14-19, dependences of higher-twist cross-sections $(\Sigma_g^{HT})^0$,

$(\Sigma_g^{HT})^{res}$, ratios $(\Sigma_g^{HT})^{res}/(\Sigma_g^{HT})^0$, $(\Sigma_g^{HT})^{res}/(\Sigma_g^{HT})^{PMC}$ and $(\Sigma_g^{HT})^{res}/(\Sigma_g^{LT})$ for processes $\pi^+ p \to gX$ and $\pi^- p \to gX$ are displayed as a function of the rapidity of the gluon y at $p_T = 4.9\ GeV/c$. For full analysis in Table II, we present numerically values of the ratio $(\Sigma_g^{HT})^{res}/(\Sigma_g^{HT})^{PMC}$ as a function of the rapidity of the gluon y at $p_T = 4.9\ GeV/c$.

Angular distributions in the higher-twist cross sections $(\Sigma_g^{HT})^0$, $(\Sigma_g^{HT})^{res}$ for processes $\pi^{\pm} p \to gX$ are presented in Figs. 20-23. As is seen from the figures, cross-sections vary slowly and smoothly with the angle of the scattering. However, angular distributions are very sensitive to the choice of the pion distribution amplitude.

As is seen from Figs.5 and 15, and also from Tables I and II, the magnitude of the higher-twist cross-section calculated by running coupling constant approach in common is enhanced by about 0.5-1 order of magnitude relative to the PMC cross-sections (cross-section is calculated in the principle of maximum conformality approach). Main reason for this is depend from phenomenological factors. As noted above in the exclusive processes the coupling constant runs not only due to loop integration, but also because of the integration in the process amplitude over the longitudinal momentum fractions of hadron constituents. Thus, the exclusive processes have two independent sources of power corrections to their characteristics; the loop integration and the integration over the longitudinal momentum fractions of quarks and gluons. It is worth noting that the latter source exists even at the leading order of pQCD, when the amplitude of the exclusive process depends on α_s. PMC scheme as is fixed factorization scheme and differ from frozen scheme with factor $e^{-5/3}$. But, in the running coupling constant approach all contributions from quark and gluon line to the cross-section must be taken into account. Thus, we can conclude that the main reason of the difference between resummed cross-section (cross-section is calculated in the running coupling constant approach) and the relative PMC cross-section is more dependent on this factor. Since only leading-twist diagrams are commonly considered in the usual studies of the hadron-hadron collision, in our calculations, magnitude of the leading-twist cross-section enhanced frozen, PMC and resummed cross-sections. But, the magnitude is the resummed cross-section the relative PMC cross-section is more near to the leading-twist cross-section. Therefore, resummed cross- section is more reliable.

Analysis of our calculations shows that $(\Sigma_g^{HT})^0$ and $(\Sigma_g^{HT})^{res}$, frozen and resummed higher-twist cross- sections, and ratios are sensitive to pion distribution amplitudes as predicted in the holographic and pQCD.

We think that this feature of infrared renormalons may help theoretical interpretations of the future experimental data for the direct inclusive gluon production cross-section in the pion-proton collisions. Higher-twist cross-section obtained in our study should be observable at hadron collider.

V. CONCLUSIONS

In this study, the inclusive single gluon production is calculated via higher twist mechanism within perturbative and holographic QCD. In the calculation of the cross-sections the running and frozen coupling constant approaches are employed and infrared renormalon poles in the cross-section expression are revealed. Infrared renormalon induced divergences are regularized by means of the principal value prescription and the Borel sum for the higher twist cross-section is found. It is observed that the resummed higher-twist cross-section differs from that found using the frozen coupling approximation, especially in some regions, considerably.

Concerning the study of the higher-twist contribution, it is primarily important to analyze its relative magnitude of contribution compared to the leading-twist contribution, since only leading-twist diagrams are commonly considered in usual studies of the hadron-hadron collision. However, in our studies the difference of the higher-twist results for the frozen and running coupling constant approaches have been studied with importance. The following results can be concluded from the experiments: the higher-twist contributions to single gluon production cross-section in the pion-proton collisions have important phenomenological consequences. Therefore, they will be helpful for detailed investigation of the dynamical properties of the nucleon. Also, the higher-twist gluon production cross-section in the pion-proton collisions depends on the form of the pion distribution amplitudes and may be used for future study. Moreover, the contributions of renormalon effects within holograpich QCD in these process are essential and may help to analyze experimental results. We compared frozen and resumed cross-sections of the direct gluon production in the processes $\pi^- p \to gX$ and $\pi^+ p \to gX$. Our calculations show in both cases running and frozen coupling constant approaches where the inclusive gluon production cross-section for the process $\pi^- p \to gX$ is suppress over the direct gluon production cross-section of the process $\pi^+ p \to gX$. Note that the direct gluon production spectrum can be measured with large precision, so results

obtained in this study will be helpful further tests of the hadron dynamics at large p_T. As is seen from Eqs.(2.4) and (3.7) higher-twist cross-sections in both cases are proportional to the third power of $\alpha_s(Q^2)$, but the leading-twist is linearly proportional to $\alpha_s(Q^2)$. Therefore, their ratios strongly depend on the $\alpha_s^2(Q^2)$.

The cross-section which is calculated by running coupling constant for all distribution amplitudes is enhanced by about 1-2 orders of magnitude of cross-section which is calculated by the frozen coupling constant method. As is seen from Figs. 6, 7, 10 and 11, the curves go up when p_T is greater than 25 GeV. According to our calculations, the main reason for it is the approaching to the very nearing of singularity point $x \to 1$ of the running coupling constant in this interval. Also, distinction is shown between running coupling constant and principle maximum conformality approaches.

Further investigations are needed in order to clarify the role of higher-twist effects in QCD. In hadron-hadron collisions, real gluons at high transverse momentum can serve as a short distance probe of the incident hadrons. Especially, the future experimental measurements will provide further tests of the dynamics of large-p_T hadron production beyond the leading twist.

Acknowledgments

One of the authors, A. I. Ahmadov is grateful to Prof. Robert Harlander and other members of the Department of Theoretical Physics University of Wuppertal for provoding hospitality extended to him in Wuppertal, where this work was carried out and to Deutscher Akademischer Austausch Dienst (DAAD) for financial support. The authors are indebted to V. M. Braun for discussions about the properties of the pion distributions amplitudes. A. I. Ahmadov is grateful for the financial support Baku State University Grant No."50+50" (2014-2015). The work of C.Aydin is supported by KTU under the research project no. BAP 2013/11641. We are also grateful to A. Mustafayev for carefully reading the paper and providing useful comments.

---

[1] S. J. Brodsky, G. L. Lepage, and P. B. Mackenize, Phys. Rev. D **28**, 228 (1983).

[2] F. S. Sadykhov and A. I. Akhmedov, Russ. Phys. J. **38**, 513 (1995).

[3] A. I. Ahmadov, I. Boztosun, R. Kh. Muradov, A. Soylu, and E. A. Dadashov, Int. J. Mod. Phys. E **15**, 1209 (2006).

[4] A. I. Ahmadov, I. Boztosun, A. Soylu, and E. A. Dadashov, Int. J. Mod. Phys. E **17**, 1041 (2008).

[5] A. I. Ahmadov, C. Aydin, Sh. M. Nagiyev, A. Hakan Yilmaz, and E. A. Dadashov, Phys. Rev. D **80**, 016003 (2009).

[6] A. I. Ahmadov, C. Aydin, E. A. Dadashov, and Sh. M. Nagiyev, Phys. Rev. D **81**, 054016 (2010).

[7] A. I. Ahmadov, R. M. Burjaliyev, Int. J. Mod. Phys. E **20**, 1243 (2011).

[8] A. I. Ahmadov, Sh. M. Nagiyev, and E. A. Dadashov , Int. J. Mod. Phys. E **21**, 1250014 (2012).

[9] A. I. Ahmadov, C. Aydin, and F. Keskin, Phys. Rev. D **85**, 034009 (2012).

[10] A. I. Ahmadov, C. Aydin, and F. Keskin, Ann. Phys. **327**, 1472 (2012).

[11] A. I. Ahmadov, C. Aydin, and O. Uzun, Phys. Rev. D **87**, 014006 (2013).

[12] A. I. Ahmadov, C. Aydin, and O. Uzun, Phys. Rev. D **89**, 014018 (2014).

[13] J. A. Bagger and J. F. Gunion, Phys. Rev. D **29**, 40 (1984).

[14] A. Bagger and J. F. Gunion, Phys. Rev. D **25**, 2287 (1982).

[15] V. N. Baier and A. Grozin, Phys. Lett.B **96**, 181 (1980).

[16] S. Gupta, Phys. Rev. D**24**, 1169 (1981).

[17] S. S. Agaev, Phys. Lett.B **360**, 117 (1995); **369**, 379(E) (1996).

[18] G.'t. Hooft, in The Whys of Subnuclear Physics, Erice, 1977, edited by A. Zichichi (Plenum, New York, 1979), p.94.

[19] A. H. Mueller, Nucl. Phys.B **250**, 327 (1985).

[20] A. H. Mueller, Phys. Lett. **B 308**, 355 (1993).

[21] V. I. Zakharov, Nucl. Phys.B **385**, 452 (1992).

[22] M. Beneke, Phys. Rep. **317**, 1 (1999).

[23] W. Greiner, S. Schramm and E. Stein, Quantum Chromodynamics, 3rd edn.(Berlin, Springer, 2007), pp.553.

[24] H. Contopanagos and G. Sterman, Nucl. Phys.B **419**, 77 (1994).

[25] A. L. Kataev, JETP Lett. **81**, 608 (2005).

[26] A. L. Kataev, Mod. Phys. Lett. **A 20**, 2007 (2005).

[27] G. L. Lepage and S. J. Brodsky, Phys. Rev. D **22**, 2157 (1980).

[28] J. F. Owens, Rev. Modern Phys. **59**, 465 (1987).

[29] E. L. Berger and S. J. Brodsky, Phys. Rev. D **24**, 2428 (1981).

[30] G. Curci, M. Greco, Y. Srivastava, Phys. Rev. Lett. **43**, 834 (1979).

[31] G. Curci, M. Greco, Y. Srivastava, Nucl. Phys. B**159**, 451 (1979).

[32] M. Greco, Phys. Lett. B **100**, 351 (1981).

[33] M. Greco, G. Penso, Y. Srivastava, Phys. Rev. D **21**, 2520 (1980).

[34] Y. I. Dokshitzer, B. R. Webber, Phys. Lett. **404**, 321 (1997).

[35] Y. I. Dokshitzer, G. Marchesini and B. R. Webber, Nucl. Phys. B **469**, 93 (1996).

[36] B. Badelek, J. Kwiecinski and A. Stasto, Z. Phys.C **74**, 297 (1997).

[37] M. Ciafaloni, D. Colferai, G. P. Salam, A. M. Stasto, Phys. Rev. D **66**, 054014 (2002).

[38] A. V. Kotikov, A. V. Lipatov, N. P. Zotov,JETP **101**, 811 (2005).

[39] C. D. Roberts and A. G. Williams, Prog. Part. Nucl. Phys. **33**, 477 (1994).

[40] S. Mandelstam, Phys. Rev. D **20**, 3223 (1979).

[41] N. Brown and M. R. Pennington, Phys. Rev. D **38**, 2266 (1988).

[42] N. Brown and M. R. Pennington, Phys. Rev. D **39**, 2723 (1989).

[43] J. M. Cornwall, Phys. Rev. D **26**, 1453 (1982).

[44] R. Alkofer and L. von Smekal, Phys. Rep. **353**, 281 (2001).

[45] L. von Smekal, A. Hauck, and R. Alkofer, Ann. Phys. (N.Y.)**267**, 1 (1998).

[46] G. Parisi and R. Petronzio, Phys.lett.B **95**, 51 (1980).

[47] J. Schwinger, Phys.Rev. **127**, 324 (1962).

[48] G. P. Lepage and S. J. Brodsky, Phys. Lett.B **87**, 359 (1979).

[49] A. Vega, I. Schmidt, T. Branz, T. Gutsche, V. Lyubovitskij, Phys. Rev. D **80**, 055014 (2009).

[50] S. J. Brodsky and G. F. de Teramond, Phys. Rev. D **77**, 056007 (2008).

[51] S. J. Brodsky, Proc. Sci., LHC07 (2007) 002.

[52] V. L. Chernyak and A. R. Zhitnitsky, Phys. Rep. **112**, 173 (1984).

[53] A. P. Bakulev, S. V. Mikhailov and N. G. Stefanis, Phys. Lett, **B 578**, 91 (2004).

[54] A. P. Bakulev, S. V. Mikhailov, A. V. Pimikov, and N. G. Stefanis, Phys. Rev. D **86**, 031501 (2012).

[55] S. S. Agaev, V. M. Braun, N. Offen, F. A. Porkert, Phys. Rev. D**86**, 077504 (2012).

[56] S. Uehara et al. [Belle Collaboration], Phys. Rev. D **86**, 092007 (2012).

[57] E. L. Berger, Phys. Rev. D **26**, 105 (1982).

[58] J. Zinn-Justin, Phys. Rept. **70**, 109 (1981).

[59] A. Erdelyi, Higher Transcendental Functions, Vol.2 (McGraw-Hill, New York, 1953).

[60] S.-i Nam, Phys. Rev. D **86**, 074005 (2012).

[61] A. D. Martin, W. J. Stirling, R. S. Thorne, G. Watt, Eur. Phys. J. C **63**, 189 (2009).

$p_T, GeV/c$	$\frac{(\Sigma_g^{HT})^{res}_{asy}}{(\Sigma_g^{HT})^{PMC}_{asy}}$	$\frac{(\Sigma_g^{HT})^{res}_{hol}}{(\Sigma_g^{HT})^{PMC}_{hol}}$	$\frac{(\Sigma_g^{HT})^{res}_{CZ}}{(\Sigma_g^{HT})^{PMC}_{CZ}}$	$\frac{(\Sigma_g^{HT})^{res}_{BMS}}{(\Sigma_g^{HT})^{PMC}_{BMS}}$	$\frac{(\Sigma_g^{HT})^{res}_{BELLE}}{(\Sigma_g^{HT})^{PMC}_{BELLE}}$
2	0.63645	0.41676	0,5223	4,5586	1,20161
4	0.80708	1.11238	1,49909	2,47698	3,72963
6	0.83428	1.69304	2,58183	2,58954	6,73942
8	0.8428	2.19939	4,08479	2,95917	10,0357
10	0.84622	2.64643	6,37155	3,60209	13,1482
12	0.84818	3.0365	10,0184	4,64649	15,545
14	0.85958	3.3647	15,924	6,30331	16,9558
16	0.85075	3.62063	25,1232	8,80723	17,5175
18	0.8518	3.78841	37,3196	12,0757	17,6427
20	0.8528	3.84589	47,2563	14,8965	17,795
22	0.85377	3.76309	45,3689	14,9752	18,3262
24	0.85471	3.49973	31,618	11,9484	19,2869
26	0.85565	3.00164	17,2571	8,38829	19,8528
28	0.85658	2.19545	8,3118	6,32575	17,4478
30	0.85752	0.98074	3,84996	7,25441	10,4326

TABLE I: Numerically value of the ratio $(\Sigma_g^{HT})^{res}/(\Sigma_g^{PMC})$ in the process $\pi^+ p \to gX$ as a function of the transverse momentum of the gluon p_T at the c.m. energy $\sqrt{s} = 62.4\ GeV$.

y	$\frac{(\Sigma_g^{HT})^{res}_{asy}}{(\Sigma_g^{HT})^{PMC}_{asy}}$	$\frac{(\Sigma_g^{HT})^{res}_{hol}}{(\Sigma_g^{HT})^{PMC}_{hol}}$	$\frac{(\Sigma_g^{HT})^{res}_{CZ}}{(\Sigma_g^{HT})^{PMC}_{CZ}}$	$\frac{(\Sigma_g^{HT})^{res}_{BMS}}{(\Sigma_g^{HT})^{PMC}_{BMS}}$	$\frac{(\Sigma_g^{HT})^{res}_{BELLE}}{(\Sigma_g^{HT})^{PMC}_{BELLE}}$
-2.52	0,70335	2,75164	7,25081	0,6715	11,1351
-2.22	0,1691	0,09216	0,03577	0,11873	0,09152
-1.98	0,19788	0,08752	0,04549	0,12802	0,11118
-1.62	0,31968	0,14862	0,11516	2,05618	0,29162
-1.32	0,47399	0,26103	0,26544	14,0557	0,70125
-1.02	0,61431	0,426	0,50365	2,85089	1,3795
-0.72	0,71688	0,64321	0,82097	2,18539	2,31447
-0.42	0,78075	0,91273	1,21556	2,18544	3,50047
-0.12	0,81581	1,23771	1,71207	2,37834	4,98013
0.18	0,83309	1,62501	2,38349	2,68376	6,84887
0.48	0,84078	2,08299	3,40504	3,13548	9,20182
0.78	0,84381	2,61508	5,218	3,90202	11,9325
1.08	0,84481	3,20622	9,08747	5,47397	14,3304
1.38	0,84501	3,79647	19,0914	9,30134	15,1705
1.68	0,84512	4,23116	43,7879	18,109	14,504
1.98	0.84586	4,16763	43,1949	19,44	14,7382
2.28	0,84847	2,90664	9,06416	7,92783	15,0257
2.52	0,9112	1,9231	8,9012	6,9834	16,2354

TABLE II: Numerically values of the ratio higher-twist cross sections $(\Sigma_g^{HT})^{res}/(\Sigma_g^{HT})^{PMC}$ calculated by running coupling constant method and principle maximum conformality approach as a function of the rapidity of the gluon y, at the transverse momentum of the gluon $p_T = 4.9\ GeV/c$ at the c.m. energy $\sqrt{s} = 62.4\ GeV$.

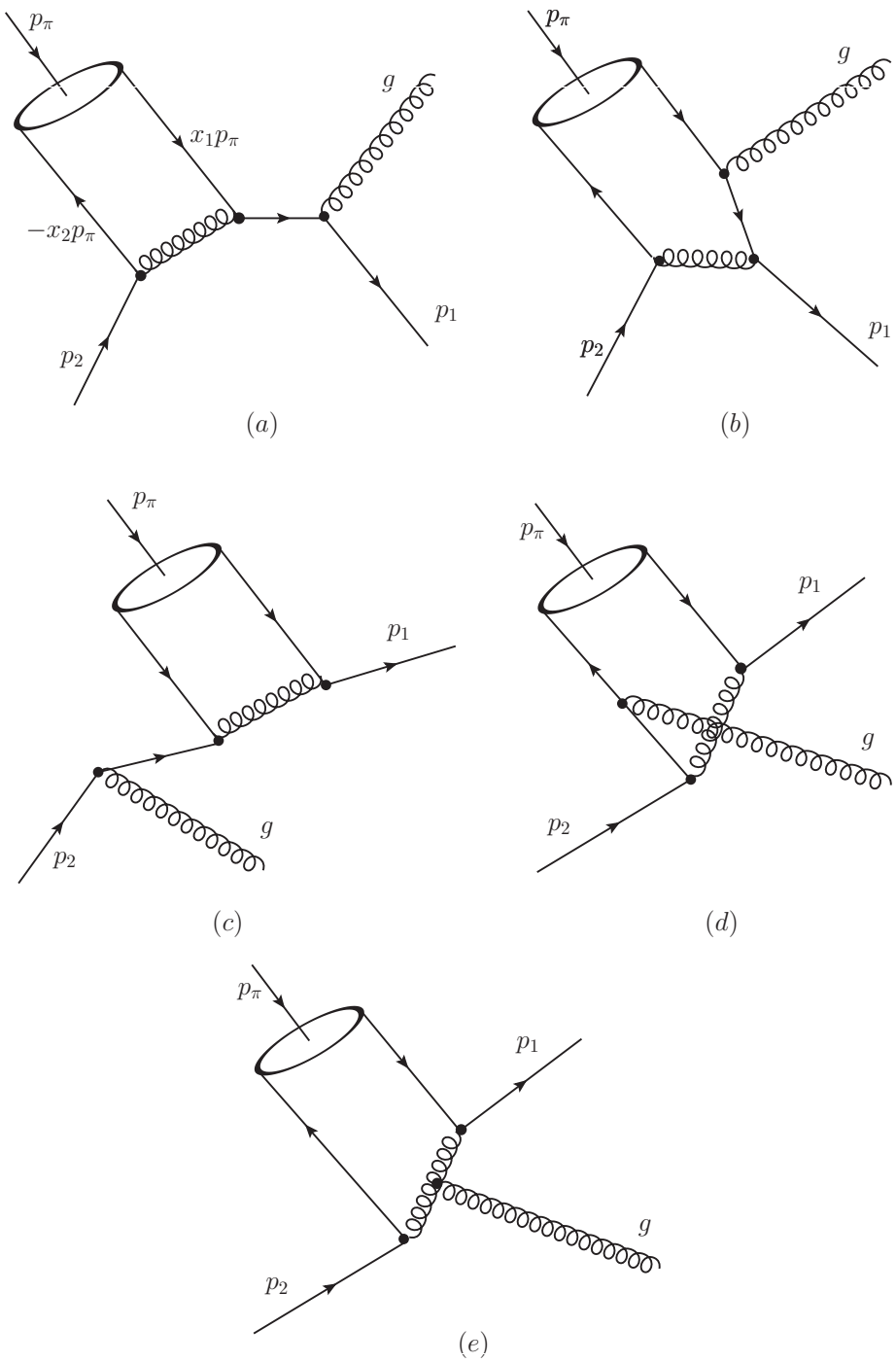

FIG. 1: Full set of QCD Feynman diagrams for higher-twist subprocess $\pi q \to gq$.

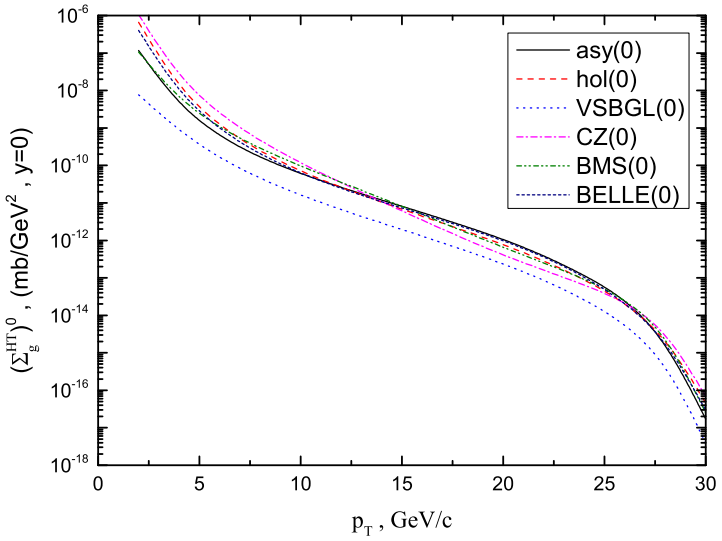

FIG. 2: Higher-twist $\pi^+ p \to gX$ inclusive gluon production cross-section $(\Sigma_g^{HT})^0$ as a function of the transverse momentum of the gluon p_T at the c.m. energy $\sqrt{s} = 62.4\ GeV$.

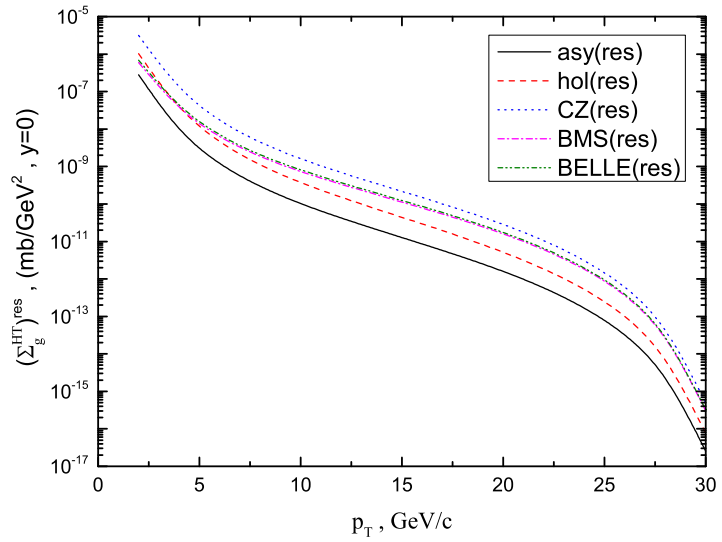

FIG. 3: Higher-twist $\pi^+ p \to gX$ inclusive gluon production cross-section $(\Sigma_g^{HT})^{res}$ as a function of the transverse momentum of the gluon p_T at the c.m.energy $\sqrt{s} = 62.4\ GeV$.

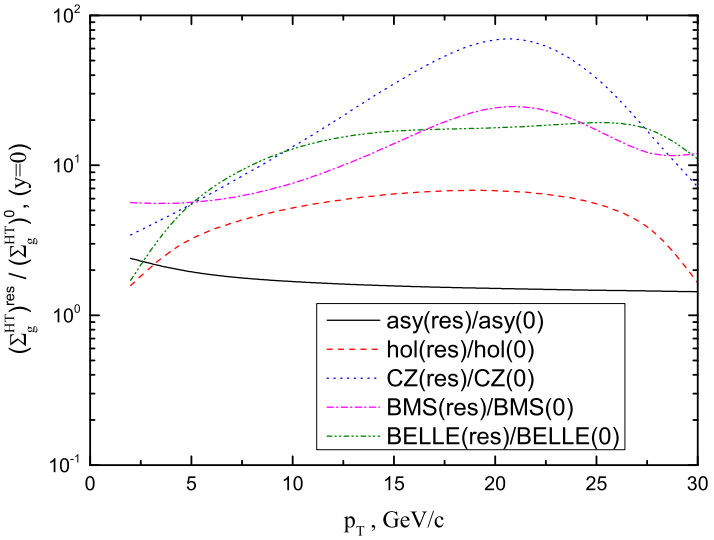

FIG. 4: Ratios $(\Sigma_g^{HT})^{res}/(\Sigma_g^{HT})^0$, in the process $\pi^+ p \to gX$, where higher-twist contribution are calculated for the gluon rapidity $y = 0$ at the c.m.energy $\sqrt{s} = 62.4\ GeV$ as function of the gluon transverse momentum, p_T.

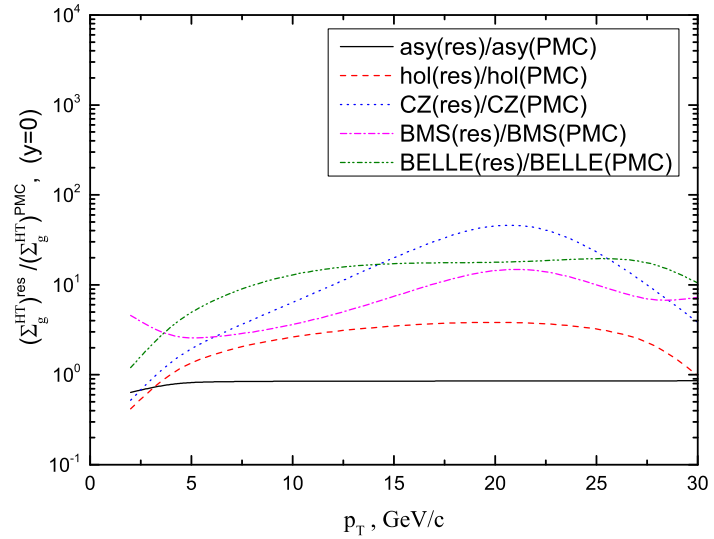

FIG. 5: Ratios $(\Sigma_g^{HT})^{res}/(\Sigma_g^{PMC})$ for the process $\pi^+ p \to gX$ as function of the transverse momentum of the gluon at the c.m. energy $\sqrt{s} = 62.4\ GeV$.

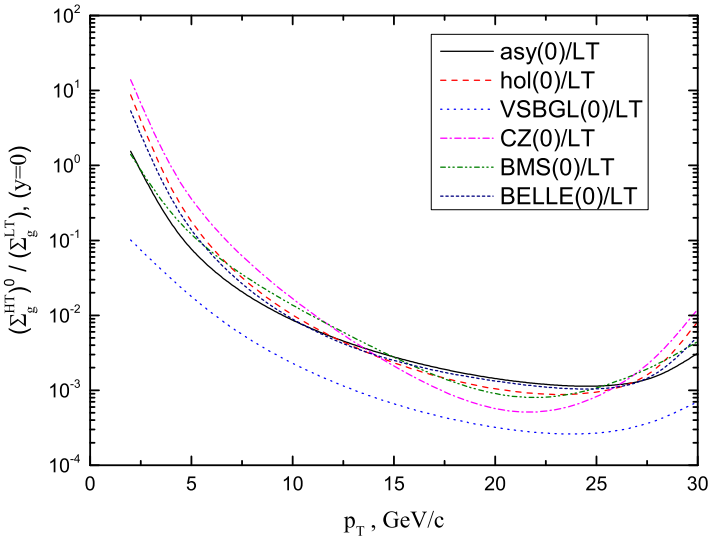

FIG. 6: Ratios $(\Sigma_g^{HT})^0/(\Sigma_g^{LT})$ for the process $\pi^+ p \to gX$ as function of the transverse momentum of the gluon at the c.m. energy $\sqrt{s} = 62.4\ GeV$.

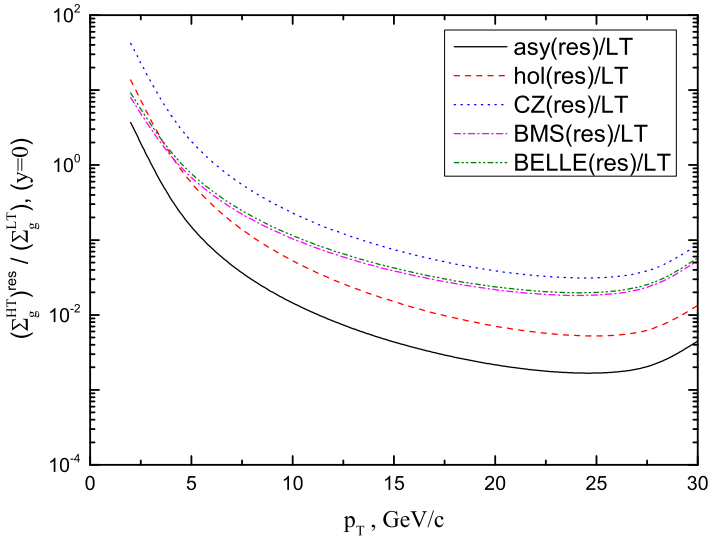

FIG. 7: Ratios $(\Sigma_g^{HT})^{res}/(\Sigma_g^{LT})$, in the process $\pi^+ p \to gX$, as a function of the transverse momentum of the gluon p_T at the c.m. energy $\sqrt{s} = 62.4\ GeV$.

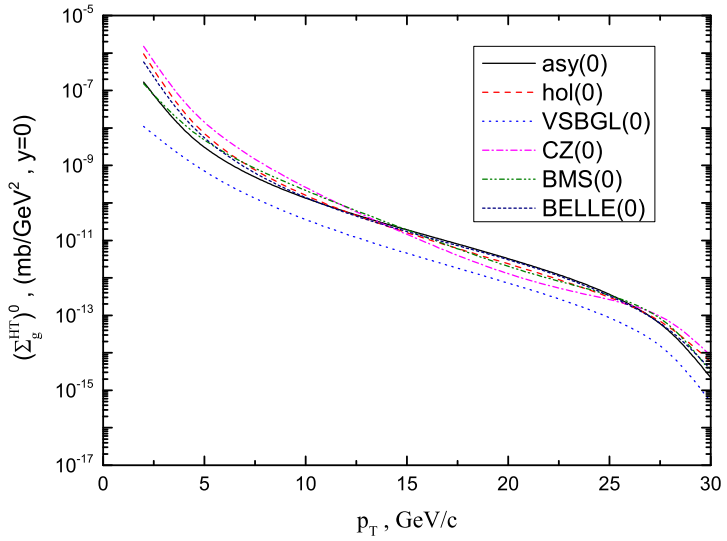

FIG. 8: Higher-twist $\pi^- p \to gX$ inclusive gluon production cross-section $(\Sigma_g^{HT})^0$ as function of the transverse momentum of the gluon p_T at the c.m. energy $\sqrt{s} = 62.4\ GeV$.

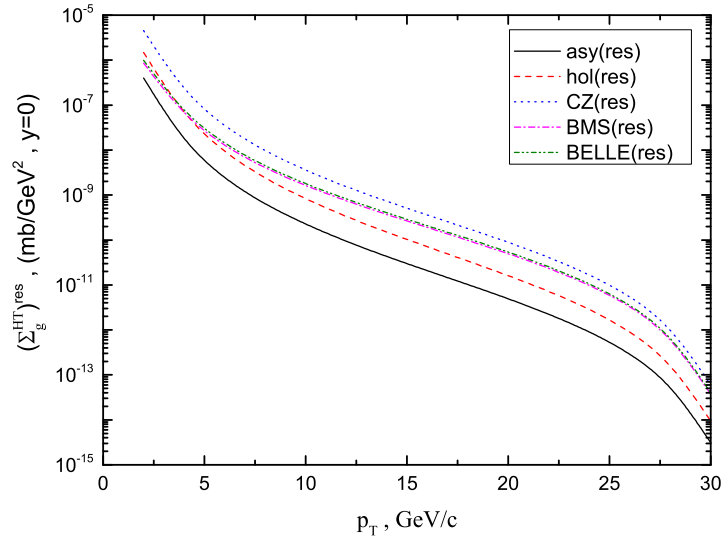

FIG. 9: Higher-twist $\pi^- p \to gX$ inclusive gluon production cross-section $(\Sigma_g^{HT})^{res}$ as function of the transverse momentum of the gluon p_T at the c.m.energy $\sqrt{s} = 62.4\ GeV$.

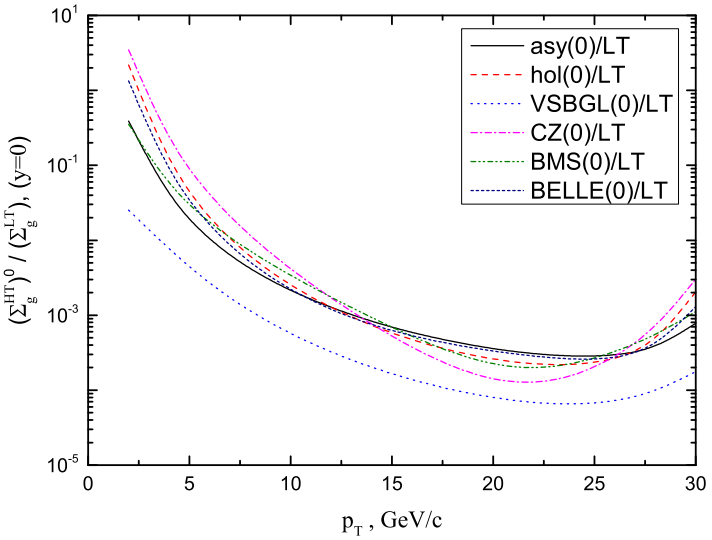

FIG. 10: Ratio $(\Sigma_g^{HT})^0/(\Sigma_g^{LT})$, in the process $\pi^- p \to gX$, as function of the p_T transverse momentum of the gluon at the c.m. energy $\sqrt{s} = 62.4\ GeV$.

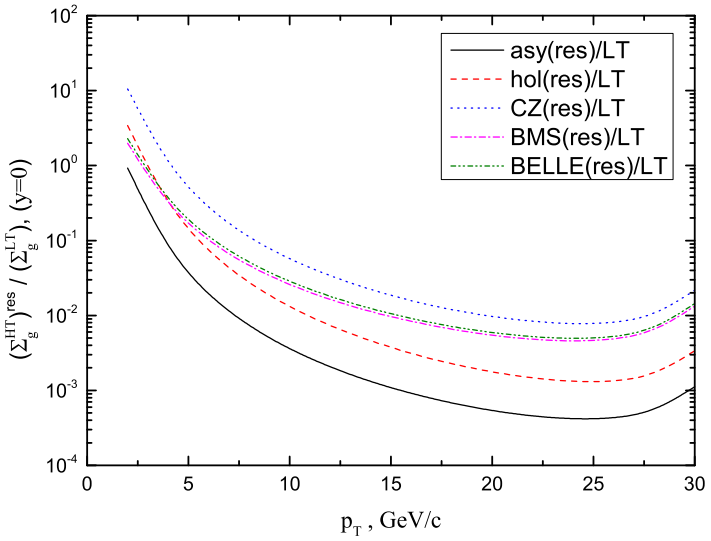

FIG. 11: Ratio $(\Sigma_g^{HT})^{res}/(\Sigma_g^{LT})$, in the process $\pi^- p \to gX$, as function of the transverse momentum of the gluon p_T at the c.m. energy $\sqrt{s} = 62.4\ GeV$.

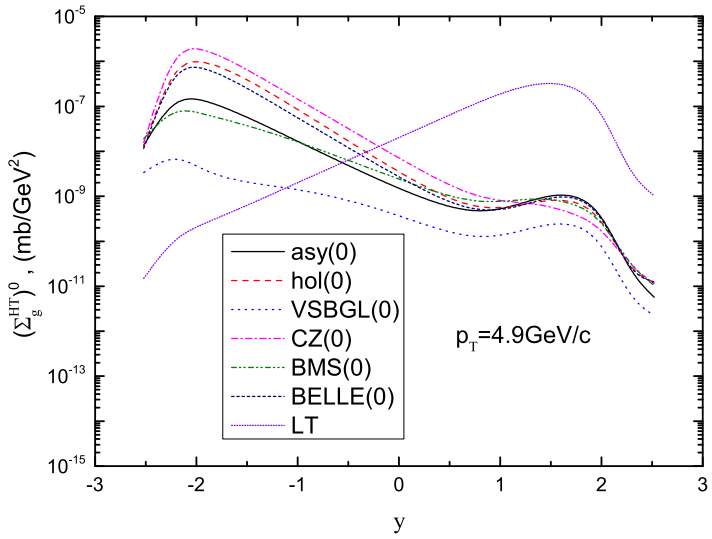

FIG. 12: Higher-twist $\pi^+ p \to gX$ inclusive gluon production cross-section $(\Sigma_g^{HT})^0$, as function of the rapidity of the gluon y at the transverse momentum of the gluon $p_T = 4.9\ GeV/c$, at the c.m. energy $\sqrt{s} = 62.4\ GeV$.

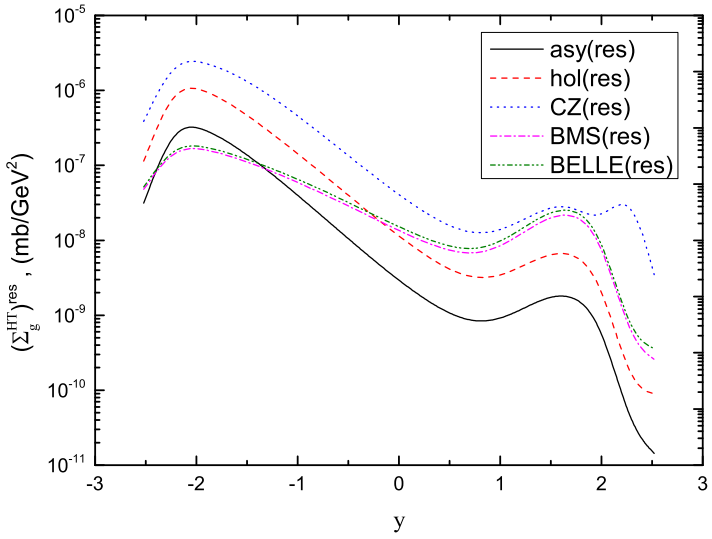

FIG. 13: Higher-twist $\pi^+ p \to gX$ inclusive gluon production cross-section $(\Sigma_g^{HT})^{res}$, as a function of the rapidity of the gluon y at the transverse momentum of the gluon $p_T = 4.9\ GeV/c$, at the c.m. energy $\sqrt{s} = 62.4\ GeV$.

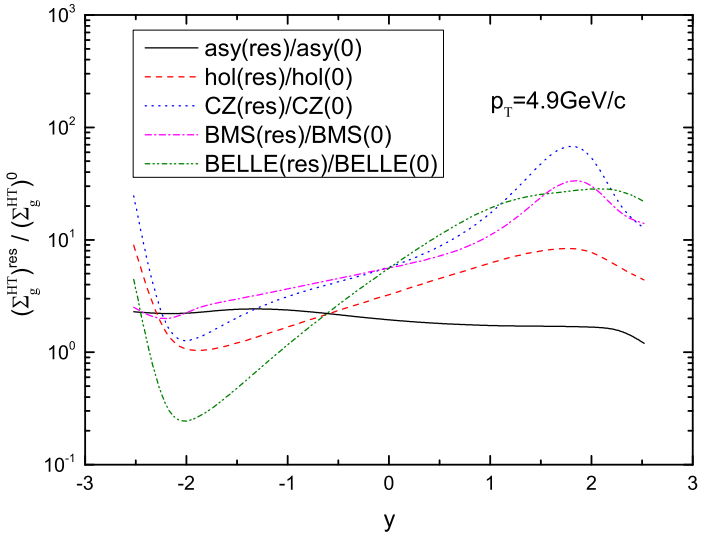

FIG. 14: Ratio $(\Sigma_g^{HT})^{res}/(\Sigma_g^{HT})^0$, in the process $\pi^- p \to gX$, as function of the rapidity of the gluon y at the transverse momentum of the gluon $p_T = 4.9\ GeV/c$, at the c.m. energy $\sqrt{s} = 62.4\ GeV$.

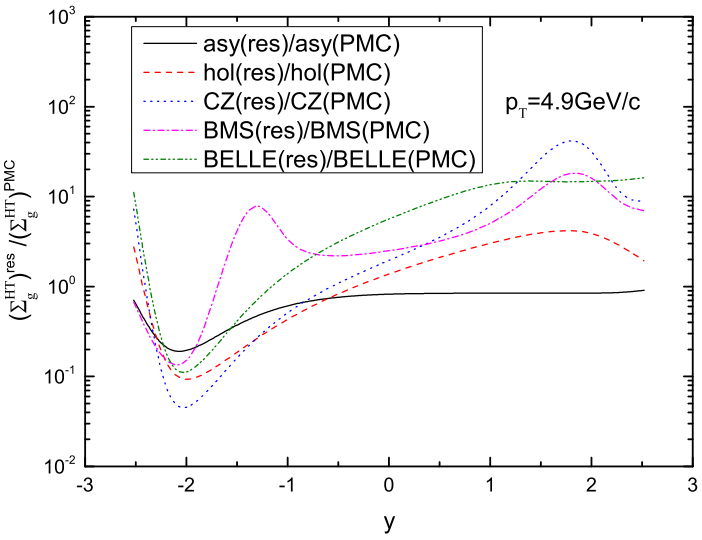

FIG. 15: Ratio $(\Sigma_g^{HT})^{res}/(\Sigma_g^{HT})^{PMC}$, in the process $\pi^- p \to gX$, as function of the rapidity of the gluon y at the transverse momentum of the gluon $p_T = 4.9\ GeV/c$, at the c.m. energy $\sqrt{s} = 62.4\ GeV$.

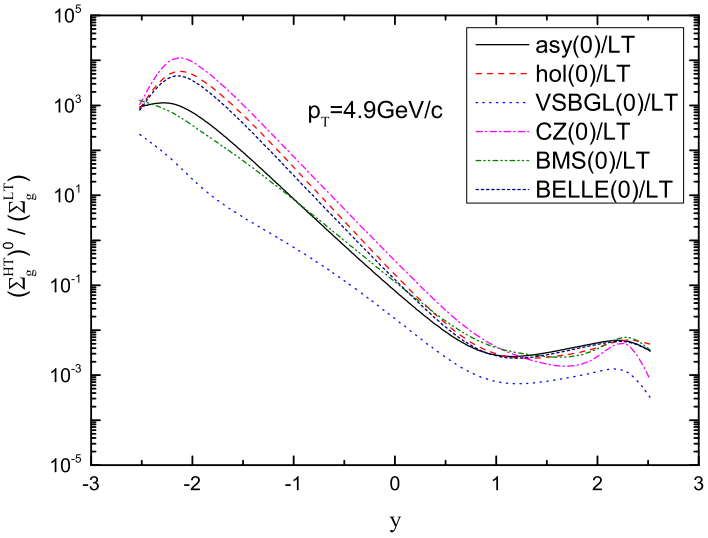

FIG. 16: Ratio $(\Sigma_g^{HT})^0/(\Sigma_g^{LT})$ in the process $\pi^+ p \to gX$, as function of the rapidity of the gluon y at the transverse momentum of the gluon $p_T = 4.9\ GeV/c$, at the c.m. energy $\sqrt{s} = 62.4\ GeV$.

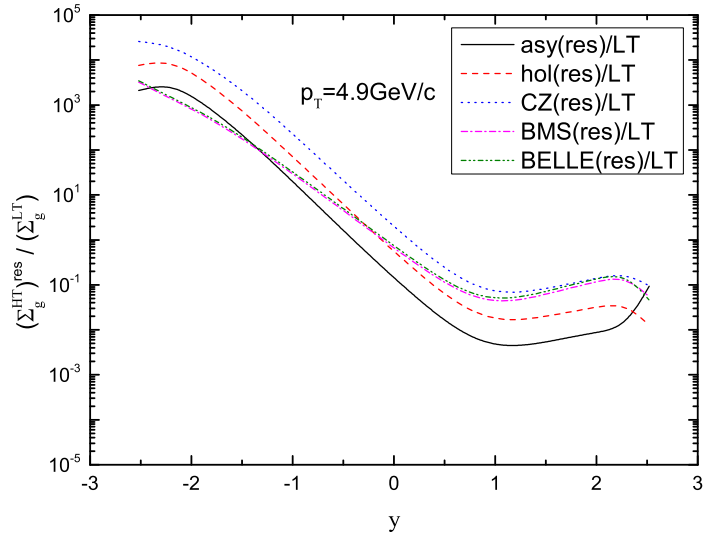

FIG. 17: Ratio $(\Sigma_g^{HT})^{res}/(\Sigma_g^{LT})$ in the process $\pi^+ p \to gX$, as function of the rapidity of the gluon y at the transverse momentum of the gluon $p_T = 4.9\ GeV/c$, at the c.m. energy $\sqrt{s} = 62.4\ GeV$.

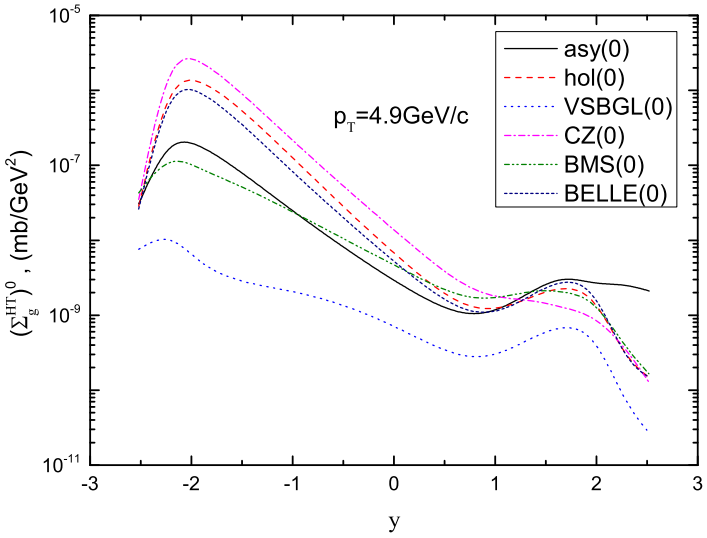

FIG. 18: Higher-twist $\pi^- p \to gX$ inclusive gluon production cross-section $(\Sigma_g^{HT})^0$, as function of the rapidity of the gluon y at the transverse momentum of the gluon $p_T = 4.9\ GeV/c$, at the c.m. energy $\sqrt{s} = 62.4\ GeV$.

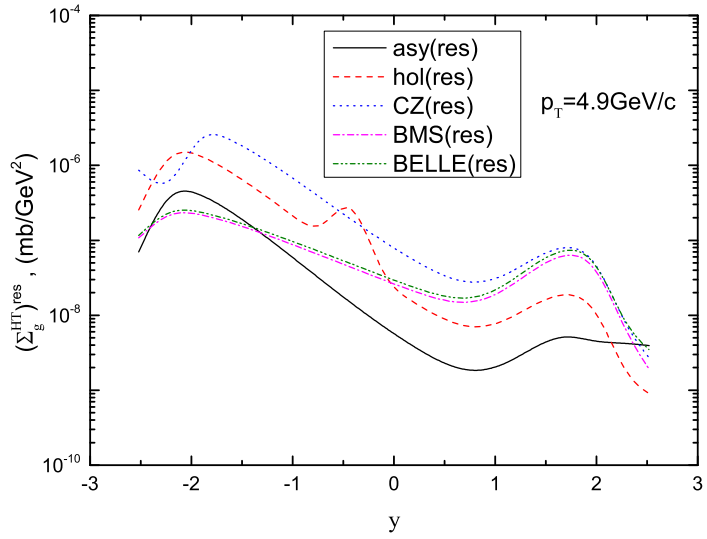

FIG. 19: Higher-twist $\pi^- p \to gX$ inclusive gluon production cross-section $(\Sigma_g^{HT})^{res}$, as a function of the rapidity of the gluon y at the transverse momentum of the gluon $p_T = 4.9\ GeV/c$, at the c.m. energy $\sqrt{s} = 62.4\ GeV$.

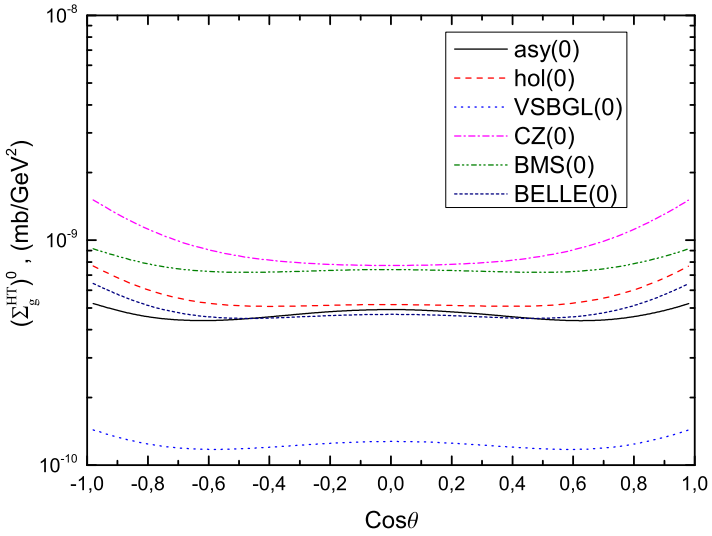

FIG. 20: Angular distributions of higher-twist cross- sections $(\Sigma_g^{HT})^0$ for the process $\pi^+ p \to gX$ at the transverse momentum of the gluon $p_T = 4.9\ GeV/c$, at the c.m. energy $\sqrt{s} = 62.4\ GeV$.

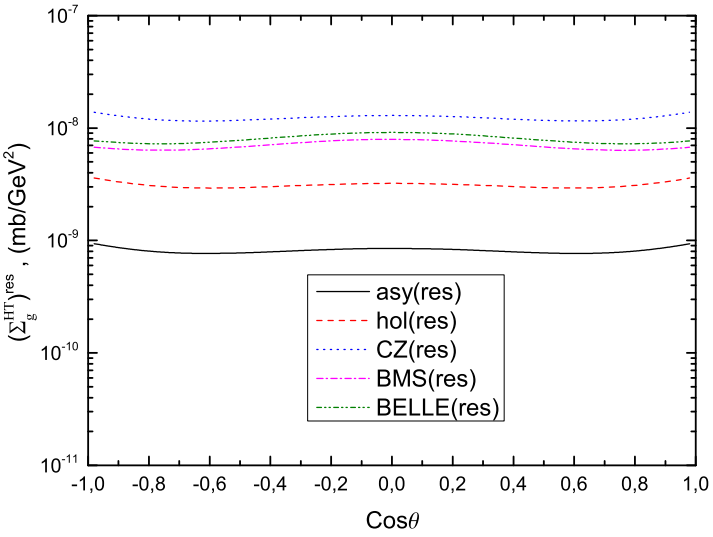

FIG. 21: Angular distributions of higher-twist cross- sections $(\Sigma_g^{HT})^{res}$ for the process $\pi^+ p \to gX$, at the transverse momentum of the gluon $p_T = 4.9\ GeV/c$ at the c.m. energy $\sqrt{s} = 62.4\ GeV$.

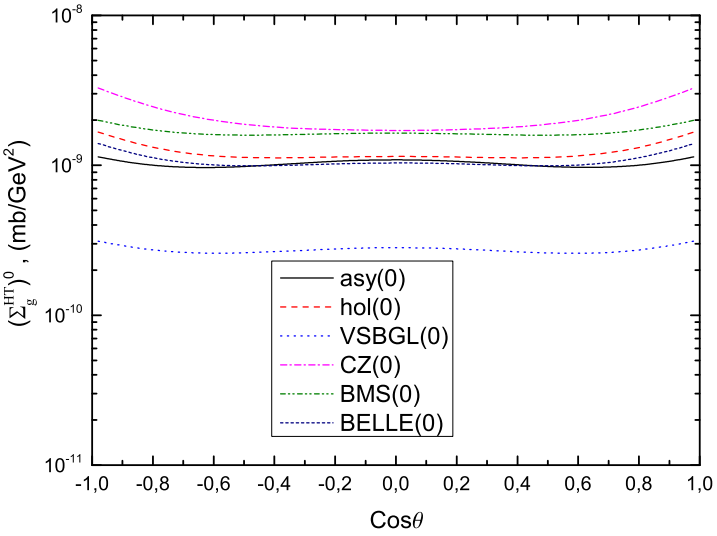

FIG. 22: Angular distribution of higher-twist cross- sections $(\Sigma_g^{HT})^0$ for the process $\pi^- p \to gX$ at the transverse momentum of the gluon $p_T = 4.9\ GeV/c$, at the c.m. energy $\sqrt{s} = 62.4\ GeV$.

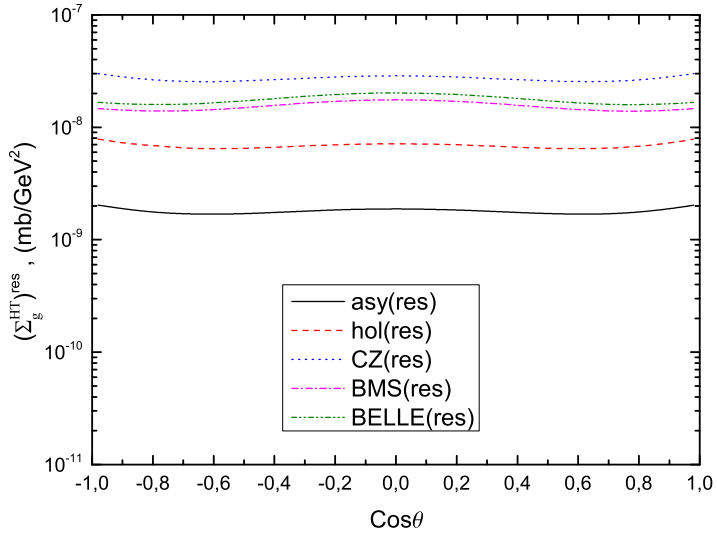

FIG. 23: Angular distributions of higher-twist cross- sections $(\Sigma_g^{HT})^{res}$ for the process $\pi^- p \to gX$ at the transverse momentum of the gluon $p_T = 4.9\ GeV/c$, at the c.m. energy $\sqrt{s} = 62.4\ GeV$.